J Therm Spray Tech (2024) 33:1040–1054
https://doi.org/10.1007/s11666-024-01750-2

ORIGINAL RESEARCH ARTICLE

SiC-YAG Coating Microstructure Optimization Through Powder Feedstock Manufacturing Process Control

D. Perello-Badia[1,2] · **N. Espallargas**[1]

Submitted: 19 October 2023 / in revised form: 9 February 2024 / Accepted: 13 February 2024 / Published online: 19 March 2024

Abstract A silicon carbide/yttrium aluminum garnet (SiC/YAG) composite powder feedstock material developed and patented by NTNU (Norway) in 2012 has been used to produce industrial SiC thermal spray coatings since 2014. This powder is the first of its kind in the thermal spray industry. The commercial powder is produced by the agglomerated and sintered route (A&S), making it suitable mostly for High-Velocity Oxygen Fuel, but it can also be produced by the sintered and crushed (S&C) manufacturing route for Atmospheric Plasma Spray (APS). In this work, a S&C route is proposed using jaw crusher, hammer mill, and ball milling techniques. The resulting powders were then deposited using APS and were compared with the reference A&S powder. The chemistry and the microstructure of the powders and coatings were characterized using electron microscopy, x-ray diffraction, and Vickers microhardness. The S&C powders showed a density higher than the A&S powder and a blocky morphology. The S&C powders had almost no internal porosity and kept the same chemical composition as the A&S version. The coatings obtained with the S&C powders outperformed the A&S coatings, having less porosity, higher hardness, and no secondary phases.

Keywords agglomerated and sintered · sintered and crushed · silicon carbide · thermal spray

✉ N. Espallargas
nuria.espallargas@ntnu.no

[1] Department of Mechanical and Industrial Engineering, Norwegian Tribology Center, Norwegian University of Science and Technology (NTNU), Trondheim, Norway

[2] Seram Coatings AS, R&D Department, Porsgrunn, Norway

Introduction

Coatings can be virtually used in any application where protection against wear (such as erosion), corrosion, high temperature, or aggressive chemicals is required, and the bulk material does not meet the specifications. Therefore, industry is constantly looking for new coating materials that can help overcome their current feedstock materials' limitations or that allow them to enter new applications and markets. The performance of thermal spray coatings depends on the composition of the coating and its microstructural characteristics. The former is influenced by the powder feedstock chemical composition, and the latter is a combination of the powder feedstock morphology and its interaction with the thermal spray method used to deposit the coatings. A deep understanding of these two factors and their influence in the final coating microstructure and performance is key to fulfill the application requirements when choosing coating materials (Ref 1).

Many new developments have been done in the field of thermal spray equipment in the last years, such as the suspension spray (HVOF or plasma), cold spraying techniques, high frequency detonation guns, and internal diameter spraying systems (Ref 1). All these developments are essential to advance industrial applications. However, advancements in new feedstock materials for thermal spray seem to go at a different pace. There are many different powder feedstock materials available with different chemical compositions and morphologies in the market. However, one that has been sought for a long time in thermal spray is silicon carbide (SiC) (Ref 2-12). Bulk SiC is used in many applications due to its properties such as high hardness, high thermal conductivity, good chemical resistance, thermal shock resistance, good wear resistance, and low density. However, SiC does not have a melting

point, which is one of the main pre-requisites for materials to be used as feedstock in thermal spray. Instead of melting, SiC sublimates at 2500 °C, therefore SiC has not been a common commercial material for thermal spray.

In 2012, a patent application, now granted in more than 60 countries, by Mubarok and Espallargas described a method to protect SiC from sublimation during thermal spraying (Ref 13-18). That method consists of using an innovative concept, where the SiC particles are covered by a protective oxide layer of yttrium aluminum garnet (YAG), making SiC thermal spray coatings possible (Ref 13). In short, that chemical method provides SiC with a melting point by covering every single SiC particle with YAG, which is later agglomerated to reach the optimal size for the spraying method. Despite this not being the first patent application about the use of SiC in thermal spray, it is indeed the first one that is commercialized under the name ThermaSiC (Ref 19). YAG was chosen as the material to protect SiC from sublimation because it is a common sintering additive in the production of SiC bulk materials, such as the liquid-phase-sintered SiC (LPS-SiC). Thermally sprayed SiC coatings open many opportunities in an industry that has been using the same feedstock materials for decades. Some of these advantages could be decreasing CO_2 emissions by reducing the aircraft engine weight by using this lighter coating material, by reducing airborne particle emissions originating from the wear of brake disks in cars and trains, by reducing maintenance costs and CO_2 emissions in the aluminum, steel, paper, and glass industry by introducing a coating that will eliminate process steps such as lubrication, among others.

Having a tangible positive impact on society through technological development is the best outcome for scientific research. This was achieved with ThermaSiC by upscaling the process from laboratory to pilot production and commercializing it since 2014 (Ref 19). Currently, ThermaSiC's first version is based on an agglomerating and sintering (A&S) route that is mostly meant for HVOF. However, the patent filed in 2012 already accounts for the sintered and crushed (S&C) route and has shown very good results at laboratory scale (Ref 13-18). New powder feedstock morphologies will bring different coating characteristics, and thus new applications and products can arise.

The aim of this paper is to establish a pilot sintered and crushed (S&C) route to expand the current spraying possibilities of ThermaSiC. This pilot S&C ThermaSiC should be better suited for plasma spray, which requires denser powders, and it is based on the original invention (Ref 13). A pre-requisite for a new powder feedstock material to reach the market safely and reliably is to have a control on the production process. Process control allows optimizing the coating microstructure for a robust coating performance. An important aspect of this research work is to understand how the different powder morphologies interact with the thermal spraying method (plasma spray) and which powder morphologies and coatings characteristics can be achieved with the S&C manufacturing process. The analysis of the coatings performance toward a final application is not the intention of this research work.

Experimental

Materials

Commercial agglomerated and sintered (A&S) powder and filtered cake were received from the pilot production site at Seram Coatings AS (Porsgrunn, Norway). Both materials were later modified: (1) The A&S powder was sieved to achieve the desired powder size distribution (see in Section "Powder Morphology, Particle Size Distribution (PSD), and Porosity"), and (2) the filtered cake was used for the S&C route testing through heat treatment, crushing, and classification. All samples consisted of 70 wt.% SiC and 30 wt.% YAG, which is equivalent in volume fraction to 84WC-16CoCr and $75Cr_3C_2$-25NiCr. The raw SiC material was purchased from Washington Mills AS (Norway) and has a composition of 4.55 wt.% SiO_2, 0.91 wt.% free C, 0.36 wt.% Fe, 0.05 wt.% Al. The filtered cake consisted of SiC particles coated with a YAG ($Y_3Al_5O_{12}$) precursor that is deposited following the process described in the patent (Ref 13). A sketch of the production route is found below (Fig. 1):

Heat Treatment of the Cake

The filtered cake received from the production site was heat treated to generate the YAG matrix for the SiC. It was first calcined and then sintered. The calcination step was performed in air atmosphere at temperatures between 500 and 800 °C depending on the dryness of the cake received. The sintering was performed at temperatures between 900 and 1650 °C in inert (Ar or N_2) atmosphere to form crystalline YAG. In this work, a Nabertherm LH-1200 °C furnace was used for calcination, and an Across International GCF 1700 muffle furnace was used for sintering. All heat treatments were performed with a heating ramp of 150 °C/h at different dwelling times (between 30 min and 5 h).

Crushing

For this work, several crushing methods, alone or in combination, were tested, i.e., ball mill, hammer mill, and jaw crusher. Two different approaches to obtain S&C powder were used. In the first approach, the material was

Fig. 1 Production route

densified in bulk and then crushed, as it is normally done in S&C manufacturing routes. In the second approach, a pre-crushing step was introduced, where the calcined material was crushed first by ball milling and then sintered. The potential benefit of this approach is to reduce contaminants from the crushing tools because the calcined material is softer and ball milling alone is enough to obtain a smaller size of the material without the need to use harsher crushing methods such as jaw crushing or hammer milling. The method used for crushing in the second approach was jaw crusher, due to its high processing capacity. Oversized material is subjected to additional crushing to increase the yield of the process. Independently of the crushing method used, the resulting crushed material is classified between steps to remove the material that already is within specifications (< 45 µm).

The ball mill equipment used was a Pascal Engineering 180W, with a 3.6-L alumina jar. The grinding medium was a blend of different sizes of alumina balls consisting of 30% of $d = 4$ mm, 50% of $d = 1$ mm, and 20% of $d = 10$ mm. The hammer mill equipment used was a MF 10 basic Microfine grinder drive with a MF 10.2 impact grinding head attached manufactured by IKA, with hammer heads made of S355 carbon steel. The jaw crusher equipment used in this work was a Retsch model B-300 equipped with stainless steel jaws and a gap setting of 1 mm. The equipment is used by many users, and it is difficult to clean, introducing the risk of contamination.

Powder Classification

The final particle size distribution of the powders was controlled by classification methods such as air sieve and mechanical sieve using standardized sieves. All particles below 25 µm are removed by air sieve to improve the efficiency on the next steps. The following classification steps are taken by mechanical sieving. The air sieve used was a Hosokawa Micron Air Jet Sieve, equipped with a Retsch 25-µm sieve. The mechanical sieve was a Retsch model Spartan, equipped with a combination of sieves that vary from 150 to 40 µm. The size of the classified powders was controlled by laser scattering particle size distribution (PSD) analysis, adjusting the sieves accordingly to obtain as similar PSD as possible between the different powders.

Table 1 Spraying parameters with APS F4MB

Parameter	Value	Unit
Spray distance	70	mm
Argon	40	l/min
Hydrogen	12	l/min
Current	600	A
Speed	66	m/min
Passes	15	…
Step	4	mm

Table 2 Summary of the powders

Powder short name	Description	Sintering temperature, °C
A&S	Representative ThermaSiC powder from the commercial A&S pilot line	1500
S&C	S&C powder, no pre-crushing	1650
S&C-HBM	S&C powder pre-crushed with hammer mill and ball mill	1650
S&C-HM	S&C powder pre-crushed with hammer mill	1650

Coating Deposition

The thermal spray coating system used to deposit coatings from the experimental and reference powder feedstocks was the Atmospheric Plasma Spray F4MB system from Sulzer Metco. The substrate material was a mild steel (S355). The parameters used are shown in Table 1, and they are the optimal for all powders in this work. No comparison with HVOF is done because the S&C powder cannot be sprayed with HVOF.

Characterization Methods

Sample Preparation

A small amount of the powder was homogeneously mixed with ground carbon resin (PolyFast, Struers) in an approximate ratio of 1:5. The mixture is then placed into a hot embedding machine, and 15 mL of carbon resin (PolyFast, Struers) is added. For the coatings, a 1-mm slice of the coatings is obtained from the middle of the sprayed sample by precision cutting. The slice is placed inside a

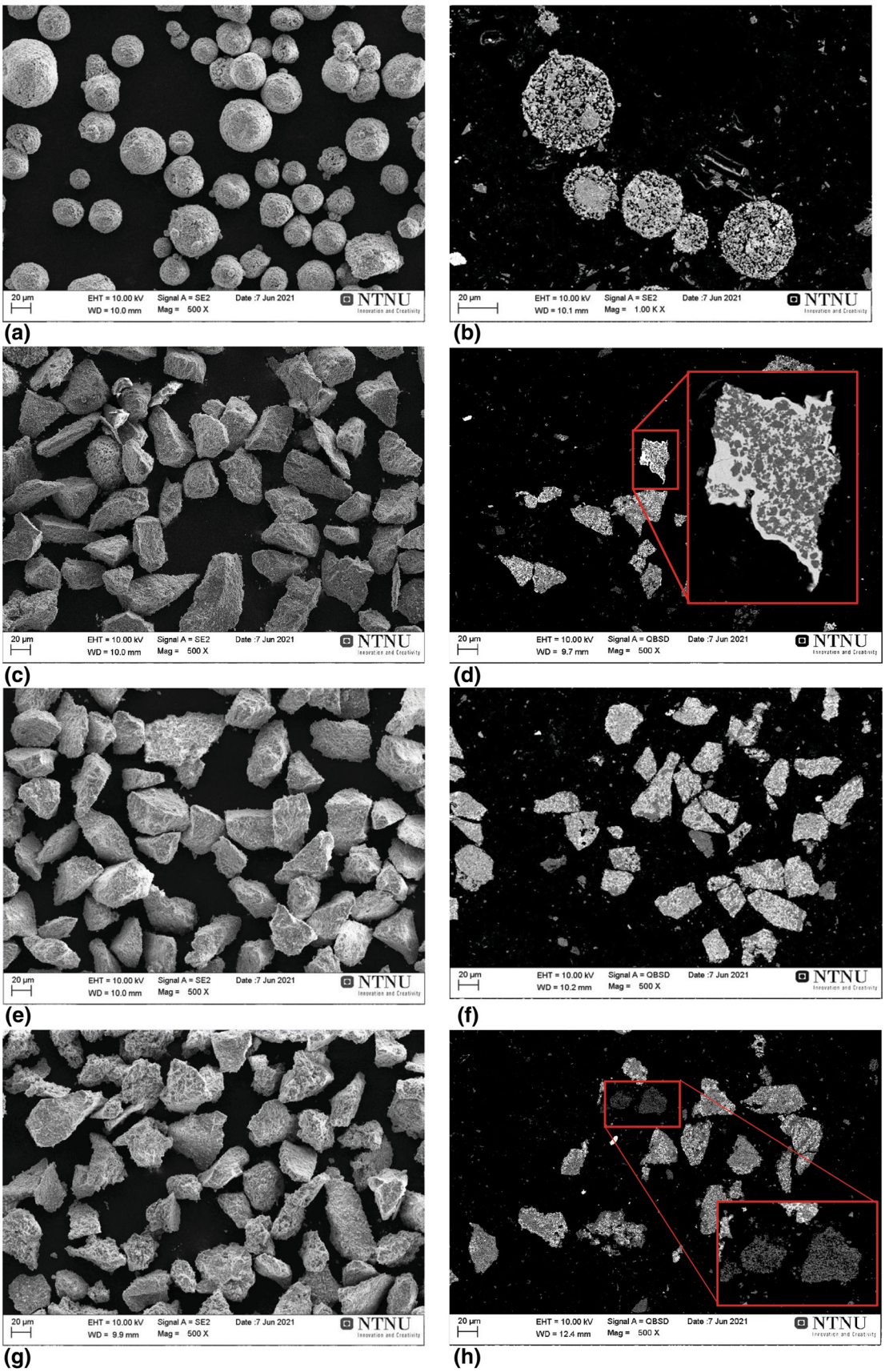
20 µm
EHT = 10.00 kV
WD = 10.0 mm
Signal A = SE2
Mag = 500 X
Date :7 Jun 2021
NTNU
(a)
20 µm
EHT = 10.00 kV
WD = 10.1 mm
Signal A = SE2
Mag = 1.00 K X
Date :7 Jun 2021
NTNU
(b)
20 µm
EHT = 10.00 kV
WD = 10.0 mm
Signal A = SE2
Mag = 500 X
Date :7 Jun 2021
NTNU
(c)
20 µm
EHT = 10.00 kV
WD = 9.7 mm
Signal A = QBSD
Mag = 500 X
Date :7 Jun 2021
NTNU
(d)
20 µm
EHT = 10.00 kV
WD = 10.0 mm
Signal A = SE2
Mag = 500 X
Date :7 Jun 2021
NTNU
(e)
20 µm
EHT = 10.00 kV
WD = 10.2 mm
Signal A = QBSD
Mag = 500 X
Date :7 Jun 2021
NTNU
(f)
20 µm
EHT = 10.00 kV
WD = 9.9 mm
Signal A = SE2
Mag = 500 X
Date :7 Jun 2021
NTNU
(g)
20 µm
EHT = 10.00 kV
WD = 12.4 mm
Signal A = QBSD
Mag = 500 X
Date :7 Jun 2021
NTNU
(h)

◀**Fig. 2** 3D SEM overview and cross-section of ready-to-spray ThermaSiC A&S commercial product (a, b), S&C powder with no pre-crushing, with detail of a particle with YAG segregation (c, d), pre-crushed S&C-BHM (e, f), and pre-crushed S&C-HM, with detail of porous particles (g, h)

holder in a vacuum chamber. Then an embedding resin (Epofix, Struers) is slowly added into the holder. The sample is then left to cure for over 12 h. All the obtained samples are polished by using an automatic polishing

Table 3 Powder particle morphology, PSD, and porosity level of the powders

Powder	PSD				Porosity, %	Powder particle morphology (N/A: not applicable)		
	*d*0, µm	*d*10, µm	*d*50, µm	*d*90, µm		Spherical	Cubic ($x/y < 0.4$)	Needle ($x/y > 0.4$)
A&S	17.37	31.38	42.53	61.53	20.19	98%	N/A	N/A
S&C	13.25	31.98	45.10	65.23	1.40	N/A	73%	27%
S&C-BHM	17.37	33.37	45.39	63.93	1.37	N/A	94%	6%
S&C-HM	15.17	31.83	44.68	64.24	4.13	N/A	89%	11%

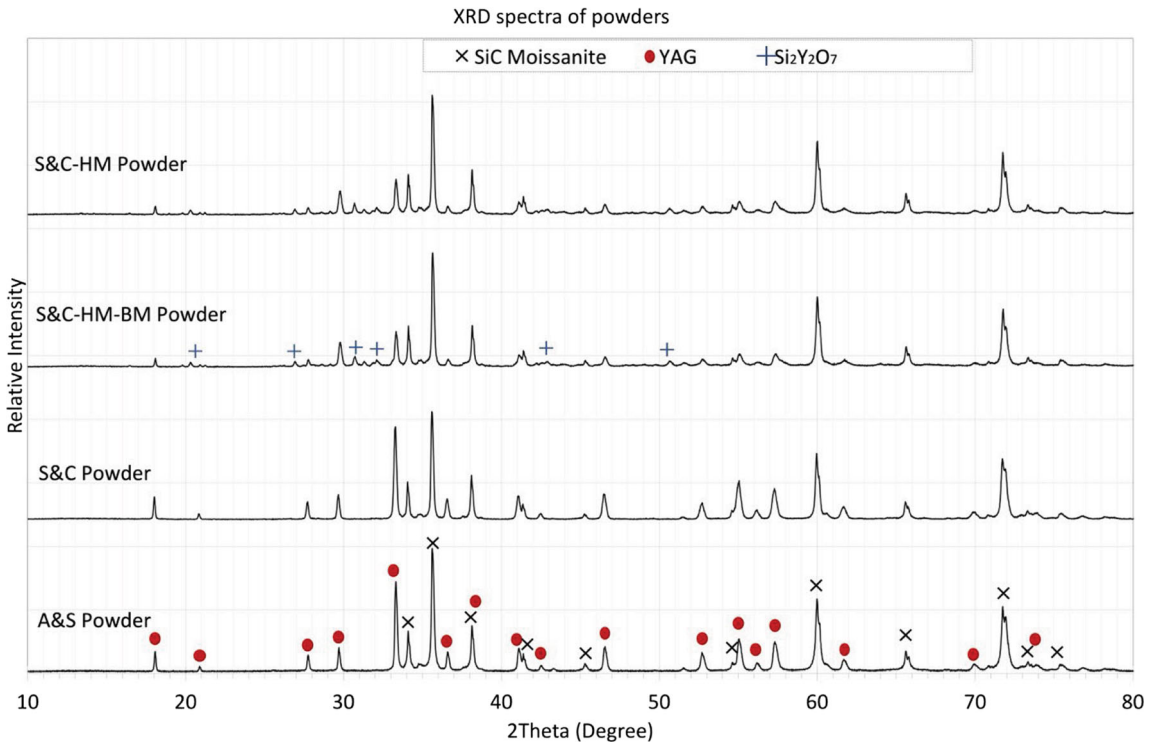

Fig. 3 XRD spectra of experimental and reference powders

Table 4 Tap density and skeletal density of the powders

Powder	Tap density, g/cm^3	Skeletal density, g/cm^3	% of theoretical density of SiC-YAG (3.615 g/cm^3), %
A&S	1.44 ± 0.01	3.43 ± 0.00	94.88
S&C	1.68 ± 0.01	3.51 ± 0.00	97.10
S&C-BHM	1.80 ± 0.02	3.53 ± 0.00	97.65
S&C-HM	1.55 ± 0.01	3.50 ± 0.00	96.82

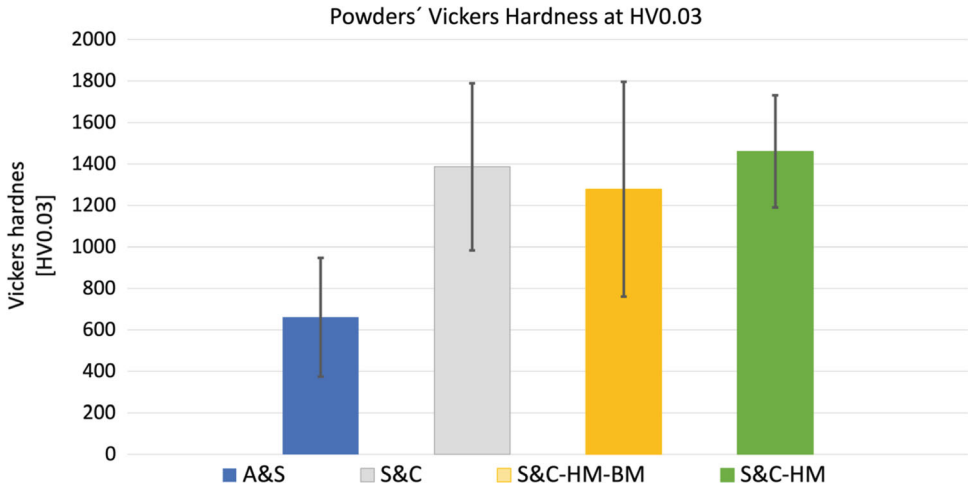

Fig. 4 Vickers hardness of powders measured at HV0.03 indenter load

machine equipped with diamond pads and finished with silica suspension.

Powder Density

Three different types of powder densities were measured in this work: tap density, apparent density, and skeletal density. Additionally, the absolute density is calculated to be used as reference. In this work, tap density was performed to powder samples using an Oulang Tap Density Volumeter, according to the ISO standard 3953:201. The bulk density of powder pellets was measured by dividing the weight by the volume. The weight was measured using a KERN 12 scale (0.05 g precision), and the volume was measured by the displacement method, where the displaced liquid after submerging the material into a graduated container was measured. The liquid used was ethanol. The skeletal density was measured by helium gas pycnometry.

Vickers Hardness

The hardness has been measured in both the powders and the coatings in the cross-section. Vickers hardness with a diamond tip shaped as a pyramid of standard dimensions was performed following the ASTM C1327-15 standard using HV0.3 indents. However, since the coatings typically have microstructural defects and variations, as the indentation load is decreased, higher hardness values are obtained. This is because at lower indentation loads, local microstructural variations have a greater influence in the hardness results. This effect has been studied in this work. Five or more (up to 10) measurements were taken for reliable hardness numbers (Ref 20).

Porosity

Porosity measurements were taken using image analysis software (ImageJ) on the SEM images of the powders and coatings. Porosity calculations by image processing are very dependent on the internal procedures of each laboratory and the subjective view of the operator performing the measurements. Porosity measurements are taken using the "threshold" and "particle analysis" tools. The "threshold" tool separates pixels by their gray scale number, by establishing a limit where all pixels with a gray value below a threshold are accounted for. In a cross-section image, the pores are darker than the coating material; thus, it is possible to separate the pores areas by their gray scale numbers. Then the selected area (pores) is transformed into "particles" and compared to the total area measured (pores plus coating), and a percentage value is given, which corresponds to the porosity value. To obtain faithful porosity values, it is important to acquire good images with enhanced contrast. This is achieved by a combination of sample preparation and image acquisition.

Particle Size Distribution (PSD)

PSD was measured by laser scattering of powder dispersed in water. The size is given by a volume-equivalent sphere diameter. The PSD of the powders was measured using a Laser Scattering Particle Size Distribution Analyzer (Horiba LA-960). The measurements were taken following the standard procedure for powders stated by Horiba, using the refractive index for SiC, as it is the most abundant phase in the powder. Each sample was measured three times, with three samples per powder, for a total of nine measurements per powder to ensure repeatability of measurements.

X-ray Diffraction (XRD)

The composition and crystallinity of the samples (powder and coatings) have been analyzed on a Bruker D8 A25 DaVinci x-ray diffractometer, using Cu Kα radiation and equipped with a LynxEye SuperSpeed Detector. The powder samples were loaded into standard holders and into Si holders for those samples with too small quantities for a standard holder. Each sample was analyzed from 20° to 80° for 30 min. The obtained crystallographic profiles were matched using the Crystallography Open Database (COD).

Microscopical Characterization

The microstructure of both powders and coatings' cross-sections has been investigated by Scanning Electron Microscopy (SEM). In this work, Secondary Electrons (SE) have been used to take the images of the different microstructures to provide with topographic information of the surface. The equipment used in this work was a FEI Quanta 650 FEG ESEM (USA).

Results

Powder Morphology, Particle Size Distribution (PSD), and Porosity

The morphology of the current commercial ThermaSiC powder is a typical A&S morphology, i.e., spherical shape and porous, as it can be observed from the SEM pictures in Fig. 1. This powder has been obtained by agglomerating the YAG-coated SiC particles with spray drying; the resulting powder is afterward sintered at 1500 °C in inert atmosphere to increase the density of the SiC-YAG particles (Ref 13).

The S&C version of this powder is not currently commercialized, but it was originally developed at laboratory scale with satisfactory results (Ref 13-18). In the S&C manufacturing route, the goal is to activate the densification mechanisms during sintering to obtain dense blocks that can be then crushed down into small particles with the optimal particle size for specific thermal spray processes. In the context of this paper, the powders were sieved to achieve similar particle size distribution. The final powder size for both S&C and A&S powders was in the range of + 30-60 µm (D_{10} and D_{90}, respectively).

Three different S&C powders are produced and are listed in Table 2. Figure 2 shows the 3D overview and cross-section of the S&C powders. The SEM images clearly show the blocky morphology of the S&C powder and the lack of porosity compared to the A&S version. All S&C powders, regardless of the pre-crushing step, showed the same morphological characteristics. In some cases, particles with a high concentration of YAG and the lack of SiC can be found (Fig. 2d). And in some particles, small isolated pores can be observed (Fig. 2h).

All powders were classified after sintering, and the detailed study of their particle morphology was performed by image analysis and PSD. The morphology types are shown in Table 3. For the reference A&S powder, the shape descriptors showed that 98% of the analyzed particles were spherical particles and 2% were non-spherical. The particles of the experimental S&C powders were all blocky and were classified in two types: cubic-like (x-axis/y-axis < 0.4) and needle-like (x-axis/y-axis > 0.4), most of the particles being cubic type (73% for powder S&C, and 94% and 89% for powders S&C-BHM and S&C-HM, respectively). The particle size distribution of the powders is represented with the values for d_0, d_{10}, d_{50}, and d_{90} also in Table 3. It can be observed that all powders show very similar values for all size fractions. The powder porosity measured with ImageJ is shown in Table 3. A clear distinction of porosity levels between the reference A&S and the experimental S&C powders was observed. The A&S powder had a relatively high porosity, in the range of 20%, and the different S&C versions had almost no porosity, with values in the range of 1-4%. These results are in accordance with the production method used for each case.

Powder Composition, Density, and Hardness

Figure 3 shows the XRD spectra for all powders. Two different chemical compositions were observed: the expected SiC-YAG composition in all powders and an additional phase ($Si_2Y_2O_7$) present in the pre-crushed powders only. In addition, the relative peak intensity of YAG was significantly smaller in the pre-crushed powders.

The tap density and skeletal density values are shown in Table 4. All experimental S&C powders were denser than the reference A&S powder. The highest tap density (1.80 g/cm^3) was measured for the S&C pre-crushed powder (S&C-BHM) and was followed by powder S&C with 1.68 g/cm^3 and powder S&C-HM with 1.55 g/cm^3. The main difference among these powders is their crushing route, with powder S&C-BHM having an additional crushing step (ball milling) than powder S&C-HM. On the other hand, the reference A&S powder shows the lowest tap density of 1.44 g/cm^3. The skeletal densities of all powders were very similar, being close to the theoretical density of the SiC-YAG (70-30 wt.%) composite material (3.615 g/cm^3). This indicates that the number of closed pores in the powders was very small.

The powders' Vickers hardness values are presented in Fig. 4, where a clear difference between the hardness of the

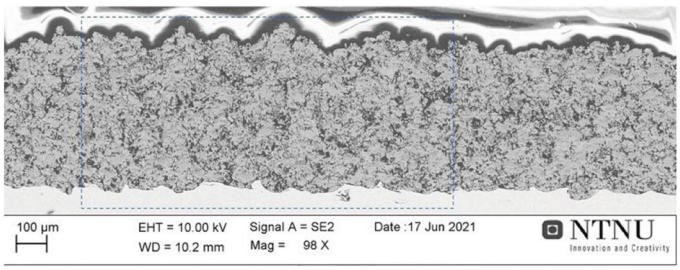
100 µm
EHT = 10.00 kV
WD = 10.2 mm
Signal A = SE2
Mag = 98 X
Date :17 Jun 2021
NTNU
Innovation and Creativity

(a)

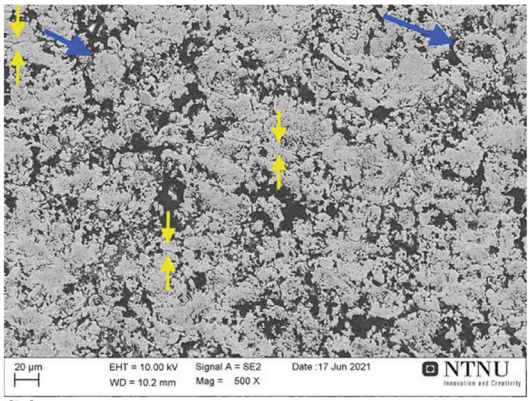
20 µm
EHT = 10.00 kV
WD = 10.2 mm
Signal A = SE2
Mag = 500 X
Date :17 Jun 2021
NTNU
Innovation and Creativity

(b)

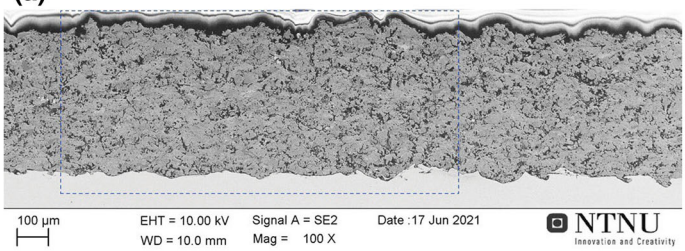
100 µm
EHT = 10.00 kV
WD = 10.0 mm
Signal A = SE2
Mag = 100 X
Date :17 Jun 2021
NTNU
Innovation and Creativity

(c)

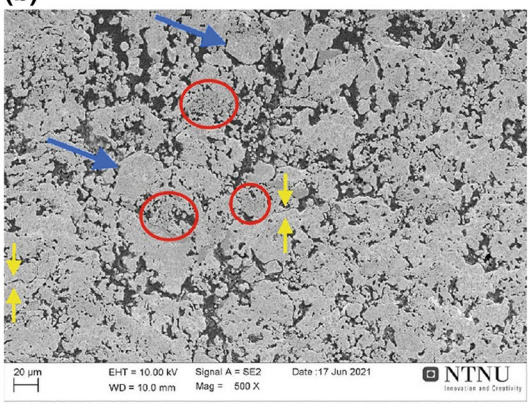
20 µm
EHT = 10.00 kV
WD = 10.0 mm
Signal A = SE2
Mag = 500 X
Date :17 Jun 2021
NTNU
Innovation and Creativity

(d)

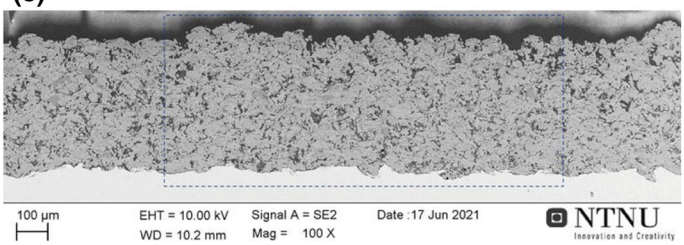
100 µm
EHT = 10.00 kV
WD = 10.2 mm
Signal A = SE2
Mag = 100 X
Date :17 Jun 2021
NTNU
Innovation and Creativity

(e)

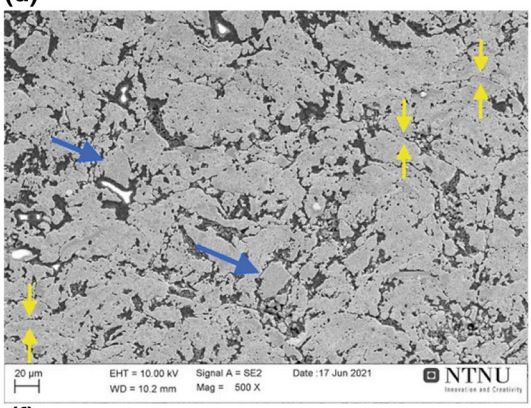
20 µm
EHT = 10.00 kV
WD = 10.2 mm
Signal A = SE2
Mag = 500 X
Date :17 Jun 2021
NTNU
Innovation and Creativity

(f)

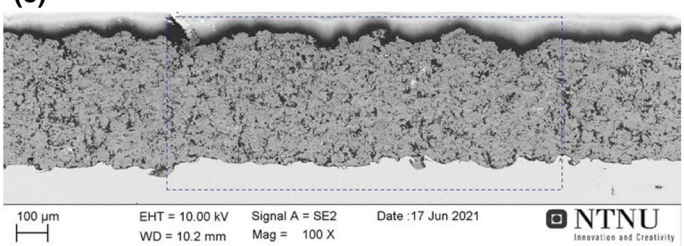
100 µm
EHT = 10.00 kV
WD = 10.2 mm
Signal A = SE2
Mag = 100 X
Date :17 Jun 2021
NTNU
Innovation and Creativity

(g)

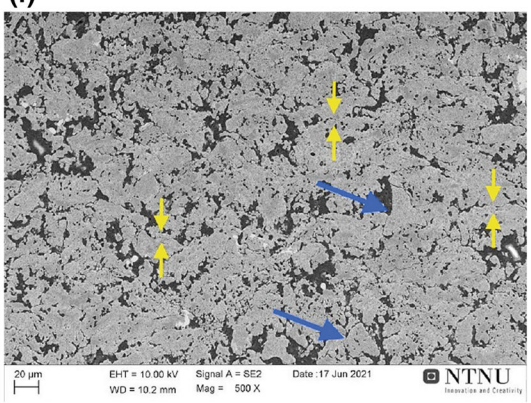
20 µm
EHT = 10.00 kV
WD = 10.2 mm
Signal A = SE2
Mag = 500 X
Date :17 Jun 2021
NTNU
Innovation and Creativity

(h)

◀**Fig. 5** SEM cross-section of the APS coatings produced with ThermaSiC A&S commercial powder (a, b), S&C powder with no pre-crushing (c, d), pre-crushed S&C-BHM powder (e, f), and pre-crushed S&C-HM powder (g, h). Blue arrows point to cold particles and yellow arrows point to interlamellar porosity (Color figure online)

reference A&S powder (ca. 660 HV) and the experimental S&C powders (ca. 1270-1470 HV) can be observed.

Coating Morphology and Composition

Figure 5 shows SEM images of the cross-section of the coatings at 100× and 500× magnification. The coatings produced with the experimental S&C powders show a denser morphology than the coatings produced with the reference A&S powder. This correlates with the measured porosity of the powders presented in Table 3. The higher-magnification images show specific microstructural features for each coating. The cold particles are indicated by blue arrows and are observed in all coatings. The interlamellar porosity is indicated by yellow arrows, and it is present in all coatings. Two types of porosity were observed in all coatings: porosity inside the lamellae and the cold particles and the porosity present between lamellae. Porosity levels were higher for the reference A&S coatings. Coating S&C-BHM showed also porous lamellae (indicated by red circles) in accordance with the porous particles seen in the S&C powder (Fig. 2d).

The XRD spectra of the coatings are presented in Fig. 6. All the coatings' XRD spectra present a broad increase in the background indicating the presence of amorphous phases. The coatings obtained with the A&S powder show small peaks of Si_2Y at 26.8°, 28.6, 34.6, 43.80, and 47.4° in addition to the SiC peaks. These peaks were not observed for the S&C coatings, where only the SiC peaks were found.

Coating Porosity, Thickness, and Hardness

The coatings' thickness and porosity are measured by image analysis, and the results are presented in Table 5. The porosity was measured using the SEM images, and it is presented as total porosity and classified by area (<10 μm^2 and > 10 μm^2), as the images used for measurements had high resolution and magnification (up to 1000×). The porosity measured for the reference A&S coatings was around 5% greater than for the S&C coatings. There is not a single method that can provide an absolute value for porosity, but rather a relative value that can be used to compare coatings as long as they are prepared and analyzed under the same conditions. Therefore, in the context of this paper, it is possible to say the A&S powder produced higher porosity coatings, which was to be expected due to the higher porosity already present in the powder. Interestingly, the porosity difference between the powder and the coatings is greater for the S&C powders, up to one order of magnitude for the coatings (see Table 3).

The hardness of the coatings is measured at different loads, and the results are presented in Fig. 7. The reference A&S coating showed the lowest hardness compared to the S&C coatings. At lower loads (HV0.03 and HV0.05), the difference in hardness between the A&S and S&C coatings is largest, and as the indentation load increases, the differences between coatings become smaller. At HV0.03, the A&S coating showed a hardness of 600 HV, whereas the S&C-BHM coating showed a hardness of ca. 1300 HV. At HV0.3, the A&S coating had a hardness of 332 HV and the S&C-BHM had a hardness of 545 HV. This is due to the fact that at higher loads, the indent is larger, and it thus takes up a larger area of the coating microstructure. The larger the area, the more porosity and other defects are taken in the measurement, and therefore, the lower the measured hardness. The trends remain very similar at all loads.

Discussion

Effect of powder composition on the sintering process

One of the main goals of this work was to develop an experimental S&C production route capable of delivering a denser powder morphology for plasma spray. A dense powder morphology is a pre-requisite for producing better coatings' microstructure in plasma spray. The powder injection in plasma spray is done directly in the jet at the outlet of the nozzle; therefore, the denser the feedstock powder, the better particle in-flight and coating morphology (see in Section "Effect of Powder Characteristics on the Microstructure of the Coatings").

The raw SiC material has a high content of SiO_2 on the SiC surface, which will be in direct contact with the YAG during the whole manufacturing process, including the sintering step. Thus, SiO_2 should be considered as one of the components in the sintering system (Ref 21). To understand the densification mechanism, the ternary phase diagram of SiO_2, Al_2O_3, and Y_2O_3 should be used as reference. This ternary system is of great interest for the liquid-phase sintering (LPS) of SiC, as Al_2O_3 and Y_2O_3 are used as sintering additives in the manufacturing process of bulk LPS-SiC products (Ref 22, 23). Typical sintering temperatures for bulk LPS-SiC products are beyond 1700 °C under inert atmosphere and high pressure. However, SiO_2 is always present on the SiC surface enhancing

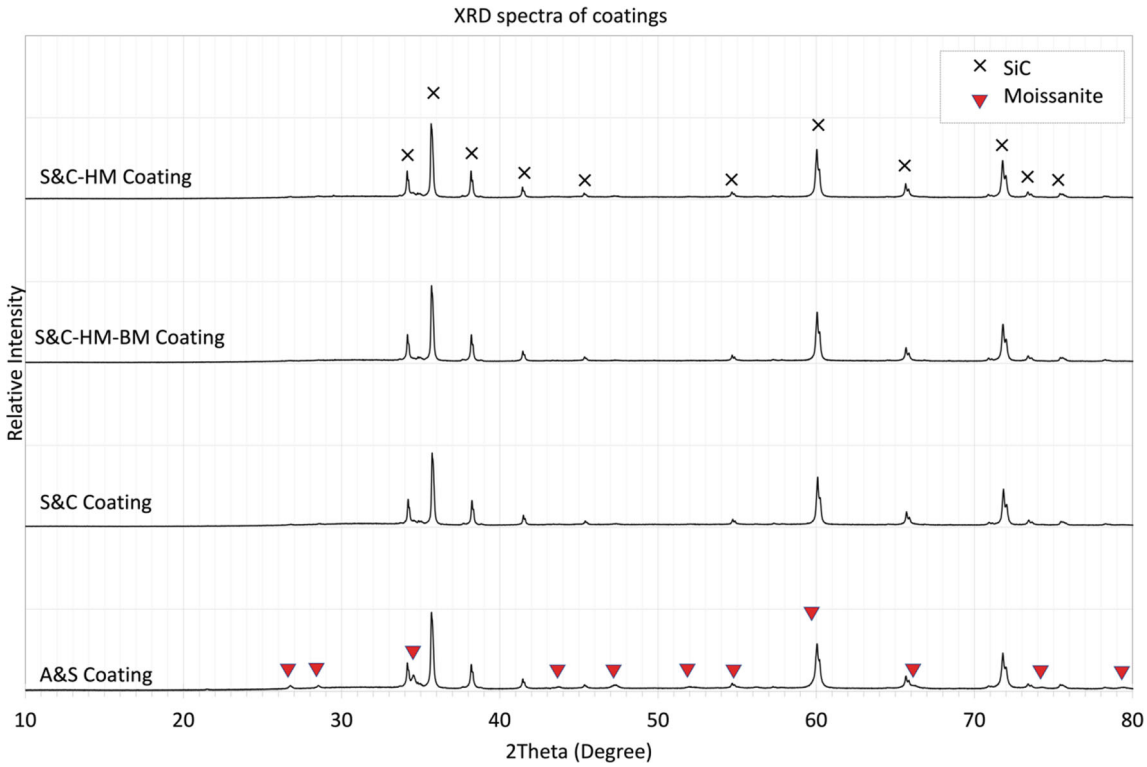

Fig. 6 XRD spectra of the coatings obtained with the different powders

Table 5 Thickness and porosity values of coatings

	Thickness, μm	Porosity, %		Total
		< 10, μm^2	> 10, μm^2	
Coating A&S	380 ± 31	2.26	18.40	21.89
Coating S&C	399 ± 14	4.64	12.34	16.54
Coating S&C-BHM	364 ± 21	2.87	13.20	16.07
Coating S&C-HM	330 ± 29	3.09	13.65	16.74

surface diffusivity and decreasing sintering temperature, and it has been studied several times as facilitator to decrease the sintering temperature of bulk SiC, being the most recent work published by Huahai Mao et al. (Ref 21). Indeed, in the work presented here, the presence of SiO_2 resulted in highly densified powders at 1650 °C, with bulk densities reaching up to 3.53 g/cm^3, which is around 97% of the theoretical density of the powder (3.62 g/cm^3, see Table 4). This indicates that there is still a 3% of closed porosity present in the sintered material. The SEM images of the cross-section of the as-sintered bulk material (Fig. 8) show two clear distinct areas: one where the YAG matrix is fully covering the SiC particles thus acting as a matrix and one where high levels of porosity and little or none YAG matrix are observed. When the porous area was studied at higher magnifications (Fig. 8b), SiC particles lacking the YAG protective layer were observed, which indicates that the precipitation of YAG precursors during the co-precipitation step was probably not optimal, leading to a heterogeneous YAG matrix distribution in the material. This could be the reason behind the ca. 3% porosity that is still present after sintering at 1650 °C. However, there are other factors to be considered, such as the lack of sintering time or even lack of sintering temperature.

In this work, we have attributed the presence of this heterogeneous YAG distribution to the YAG segregation observed in the as-sintered bulk material (Fig. 2d). Indeed, this YAG segregation is an indication of a liquid phase achieved during sintering. When the YAG reaches a liquid phase during sintering, a new transport mechanism activates, the so-called viscous flow. This mechanism transports or diffuses the viscous YAG from highly stressed areas to low stressed areas (Ref 24). This means that the viscous YAG will flow toward voids and surfaces. This

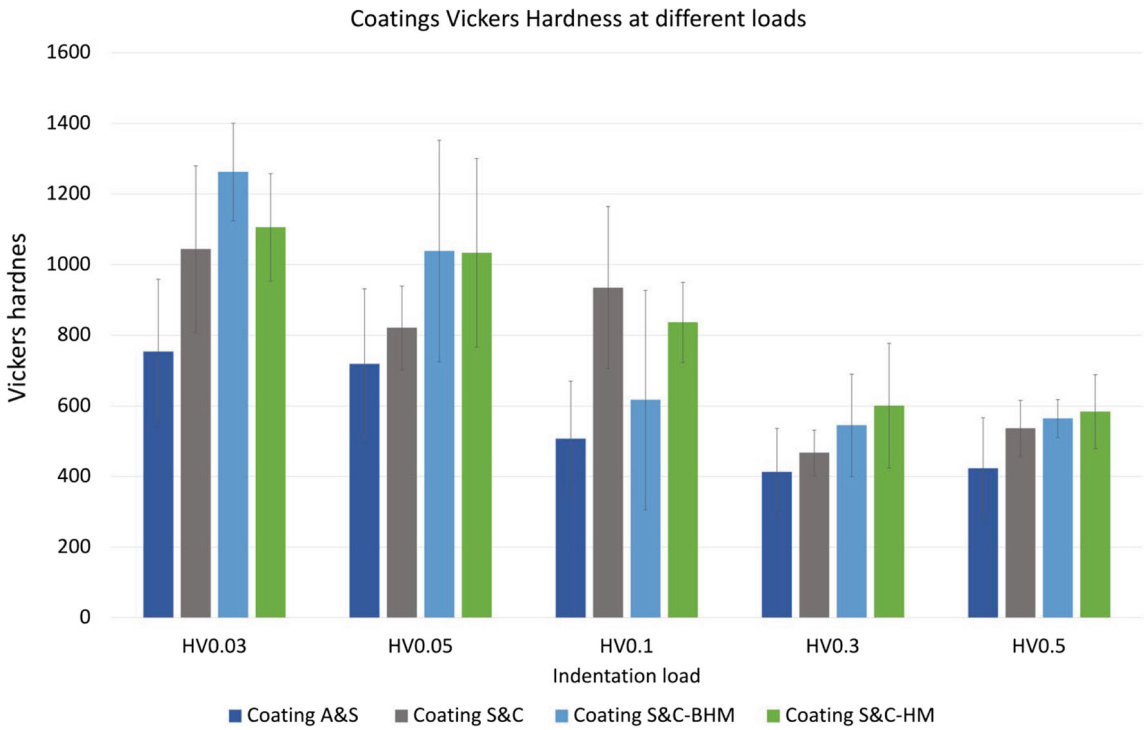

Fig. 7 Vickers hardness of the coatings at different loads

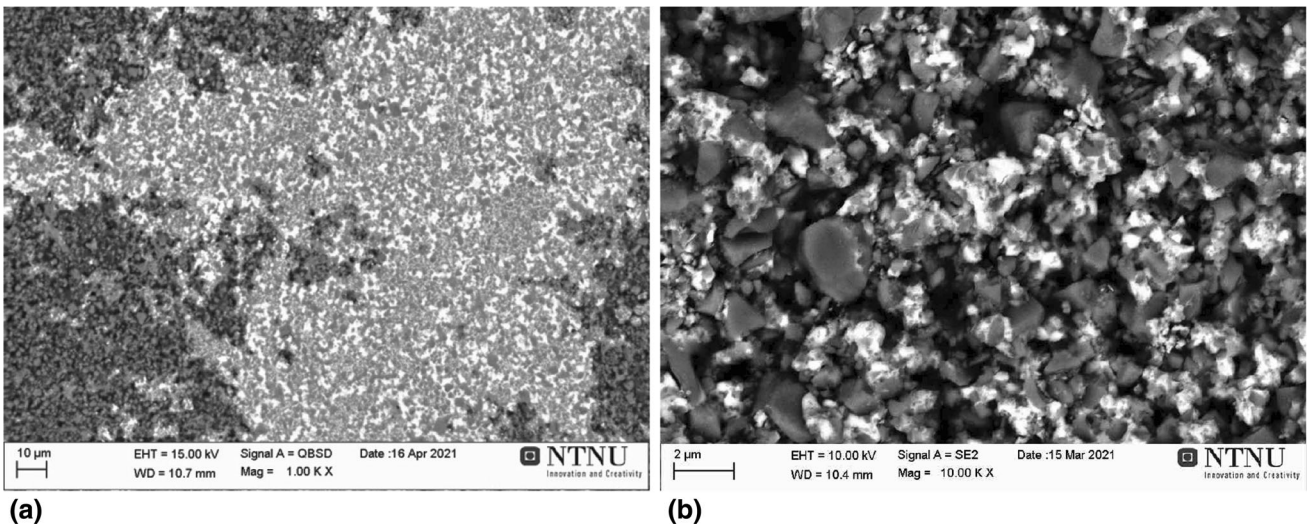

Fig. 8 SEM images of the cross-section of the as-sintered bulk material, (a) dense (bright) and porous (dark) areas and (b) unprotected SiC particles

migration will inevitably create areas with SiC clusters, as the YAG matrix leaving these areas gets thinner. This effect can be clearly seen in Fig. 9. This is indeed possible because of the SiO_2 present on the surface of the SiC particles. Thus, at a local level, the ternary system SiO_2-Al_2O_3-Y_2O_3 is heavily shifted toward the SiO_2 decreasing the liquidus temperature of YAG formation. However, this mechanism also enhances the formation of secondary phases such as $Y_2Si_2O_7$ (Fig. 3).

Effect of Pre-crushing on the Final Powder Characteristics

Two crushing approaches were tested in this work, with and without pre-crushing before sintering. The S&C material with no pre-crushing resulted in a satisfactory SiC-YAG chemical composition, since no secondary phases were found by XRD (Fig. 3), and a typical S&C morphology (Fig. 2). However, the high hardness of the

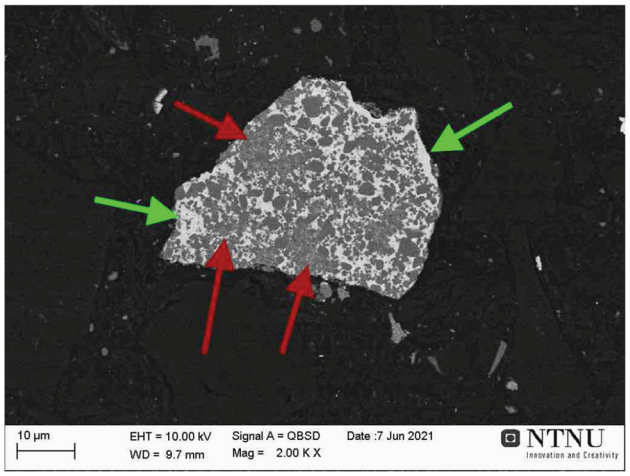

Fig. 9 Detail of high-YAG content areas (green arrows) and SiC clustering (red arrows) (Color figure online)

sintered bulk material (1474 HV) made the crushing operation challenging, wearing out the tooling material leading to low material yields, so several iterations are needed to obtain significant powder quantities. This will eventually increase the processing time and the costs of production.

On the other hand, the pre-crushed S&C materials showed, in addition to YAG, undesirable secondary phases ($Y_2Si_2O_7$) indicating that this approach is detrimental to achieve a desirable chemical composition. Although this secondary phase might provide with an advantage for the densification process (as it will be explained in Section "Influence of the Powder Secondary Phases on the Final Coating"), it brings brittleness to the coating. This secondary phase can be the result of local overheating during the crushing process. However, crushing before sintering has an advantage from a processing point of view, as the pre-crushed material is soft and does not wear as much the tooling material. Future work should be done to control this secondary phase formation because silicates and silicides are brittle phases that weaken the coating. Indeed, laboratory work performed by Mubarok and Espallargas proves that a pre-crushing step can be done without inducing secondary phase formation (Ref 14).

Different crushing processes were used in this work. The jaw crusher was not able to produce powder in the wanted range of < 45 µm. It, however, turned out to be a necessary intermediate step between the densified bulk material and the final crushing and milling steps, as it is the only method capable to accept feeding material in the size ranges of the sintered bulk material. When using the rotary hammer mill, severe wear of the carbon steel hammer heads was observed. The metallic contamination was removed using a magnet during the air sieving step. Another way of reducing this problem will be to use hammer heads made of harder materials. Powders S&C and S&C-HM were produced using the rotary hammer mill, resulting in powder tap densities of 1.68 and 1.55 g/cm^3, respectively. However, powder S&C-BHM produced by ball milling of the oversized material of powder S&C-HM resulted in a tap density of 1.80 g/cm^3. This could be explained by the different working principles of the crushing techniques. In rotary hammer mill, when the particles reach a specific mesh size, they leave the crushing chamber. On the other hand, in ball milling, the particles stay in the milling chamber until the operation is finished, being subjected to crushing forces for a longer time. As it is already discussed in Section 4.1, two distinct regions are found in the sintered bulk material: dense and porous. The dense region results in a higher hardness and can withstand the crushing forces for longer time than the porous region. The longer time used in ball milling reduces the size of the porous particles into sizes smaller than 25 µm, which was the lower mesh size used during classification, leaving a major portion of dense particles in the final powder than in the powders produced with rotary hammer mill, which leads to an increase in tap density. This can be observed in Fig. 10, where the hammer-milled material does show both dense and fully porous particles (indicated by a blue arrow), and the ball-milled material only shows fully dense particles. Therefore, ball milling should be the preferred crushing option since eliminating the porous particles contributes to more homogeneous powders with higher density and less contamination from the tooling material.

Effect of Powder Characteristics on the Microstructure of the Coatings

The reference A&S coating and the S&C coatings showed significant differences despite having both been produced with powder that presented identical chemical composition (Fig. 3). In addition, the porosity values of the S&C coatings are lower for the reference A&S coating (Table 5), and the hardness at HV0.3 is higher for the S&C coating (467 ± 65 versus 332 ± 69 $HV_{0.3}$). At lower indentation loads, the hardness differences increase, with the S&C coating reaching values of 1044 ± 236 $HV_{0.05}$ versus 599 ± 220 $HV_{0.05}$ of the reference A&S coating. The XRD spectra of the coatings (Fig. 6) show the presence of Si_2Y in the A&S coating only, indicating that the morphology of the A&S powder plays a role in the formation mechanism of this secondary phase since this phase was not observed in any of the S&C coatings. As mentioned earlier, secondary phases are not desired, especially those that can bring brittleness to the coating, such is the case of silicides and silicates. The YAG peaks are not present in any of the coatings, and instead, a broad increase in the background

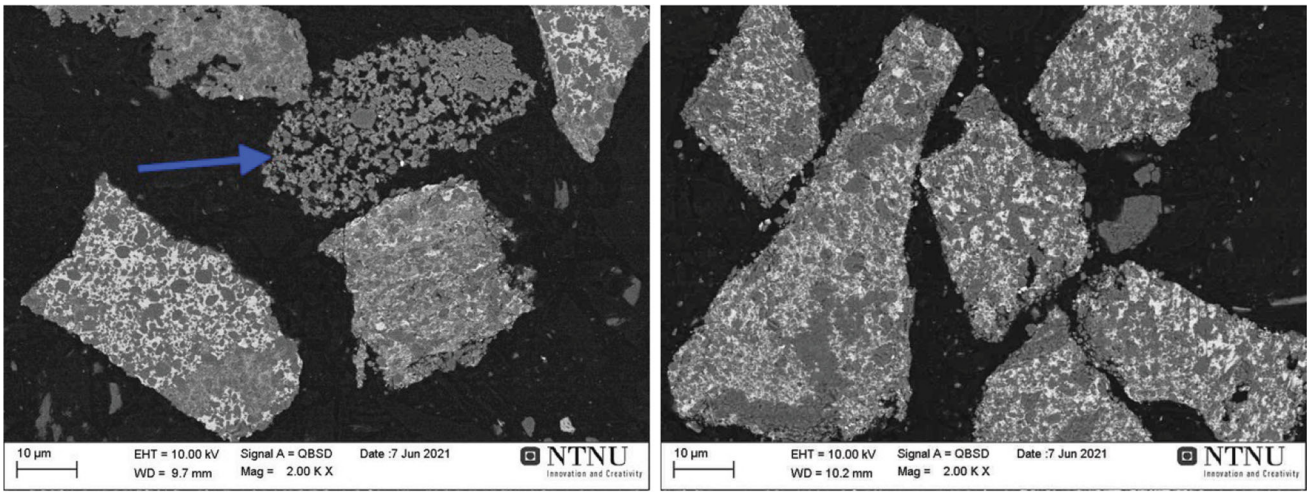

Fig. 10 SEM images of the hammer-milled (a) and ball-milled (b) powders

indicates that all YAG is in the amorphous or nanocrystalline state.

As these coatings were produced by powders with identical chemical composition, and under the same spraying conditions, the influence of SiO_2 on the particle densification in-flight can be ruled out, leaving the morphology of the powder as the only contributor to the coatings' microstructural differences. According to the in-flight particle-plume (jet) interaction theory, the S&C powders reach a higher degree of melting than the A&S version due to the following effects: (1) The lower particle porosity provides with a more effective heat transfer with the plume, (2) the higher powder density provides with longer in-flight time, (3) there is a higher effective heat transfer due to higher surface area interaction with the plasma plume (jet), and (4) the higher inertia of the denser powder particles provides with a lower deceleration after leaving the plume (jet). All these effects together contribute to a higher degree of melting of the S&C powder particles upon impact with the substrate, which in turn results in a better coating microstructure (e.g., better interlamellar cohesion and lower degree of porosity). This is in accordance with the improved coating characteristics found for the S&C coatings in this work (Table 5 and Fig. 7).

Influence of the Powder Secondary Phases on the Final Coating

To evaluate the influence of the powder secondary phases in the final coating characteristics, S&C-BHM and S&C-HM powders are chosen for comparison purposes. The XRD spectrum of powder S&C-HM shows the presence of $Y_2Si_2O_7$ in addition to YAG and SiC. $Y_2Si_2O_7$ has a melting point of 1775 °C (Ref 25), significantly lower than the melting point of YAG (1942 °C). Thus, it can be assumed that the particles with a $Y_2Si_2O_7$-YAG matrix will reach a higher degree of melting under the same spraying conditions, leading to denser coatings. This is confirmed by the porosity measurements (Table 5) and the hardness values at higher loads (HV0.3 and HV0.5). However, the wide standard deviation of the hardness measurements and the closed porosity values do not make these differences significantly enough to be conclusive, and this hypothesis should be confirmed with further experiments. All hardness measurements show a wide standard deviation, indicating the presence of local defects and heterogeneous microstructures. The decrease in coating hardness can be correlated to the local defects present in the coatings' microstructure. At lower loads, few failure mechanisms of the local defects are activated. As the load increases, more defects are activated, contributing to a decrease in the measured hardness. However, high hardness is obtained in the S&C powders and coatings at low loads, indicating that a homogeneous SiC-YAG coating microstructure with no defects could reach hardness values in the range of 2000 HV, which is typical for LPS-SiC bulk materials (Ref 26).

Conclusions

The viability of optimizing the microstructure of SiC thermal spray coatings by creating a sintered and crushed powder morphology with different production routes has been studied in this work. The SiC raw material was processed using different sintering temperatures and different crushing techniques such as hammer mill, jaw crusher, and ball milling. The obtained S&C powders and a reference

A&S powder were sprayed with Atmospheric Plasma Spray (APS) to deposit coatings under the same spraying parameters. The results have been compared, and the influence of the powder characteristics on the coating microstructures has been assessed. The following conclusions can be drawn from this work:

- The S&C route produces powders with satisfactory chemical composition and morphology that can be used as benchmark against the A&S commercial powder.
- The S&C APS coatings presented an improved hardness and porosity with respect to the reference A&S coating. The S&C powder morphology, with lower porosity, higher tap density, and higher surface area, can achieve a higher degree of melting during the deposition process, leading to denser coating microstructures.
- The microstructural properties of the coatings can be tailored to a certain degree by controlling the powder manufacturing routes and process parameters. This opens the door to new ThermaSiC coatings and therefore new applications.

Acknowledgments Open Access funding was provided by NTNU Norwegian University of Science and Technology (including St. Olavs Hospital - Trondheim University Hospital). The authors would like to thank Emil Valaker for fruitful discussions critical for this research work. The authors are grateful for the financial support from Seram Coatings AS.

Funding Open access funding provided by NTNU Norwegian University of Science and Technology (incl St. Olavs Hospital - Trondheim University Hospital).

References

1. N. Espallargas Ed., *Future Development of Thermal Spray Coatings: Types, Designs, Manufacture and Applications*, Elsevier, Amsterdam, 2015
2. B. Wielage, J. Wilden, T. Schnick, A. Wank, J. Beczkowiak, R. Schulein, H. Zoz, and H. Ren, Mechanically alloyed SiC composite powders for HVOF applications, in *International Thermal Spray Conference 2002* (2002), pp. 1088-1092.
3. B. Wielage, J. Wilden, T. Schnick, and A. Wank, Development of SiC-composite feedstock for HVOF applications, in *Thermal spray Conference 2002* (2002), pp. 790-795.
4. D. S. Gollob, T. H. Piquette, J. Derby, O. B. Al-Sabouni, R. K. Schmid, and J. C. Doesburg, *Thermal Spray Feedstock Composition* (2012).
5. H. Kang and S. Kang, Thermal Decomposition of Silicon Carbide in a Plasma-Sprayed Cu/SiC Composite Deposit, *Mater. Sci. Eng. A*, 2006, **428**(1-2), p 336-345.
6. H. Kang, Microstructures of High Volume SiC Reinforced Tungsten Composites Produced By Plasma Spray, *Scr. Mater.*, 2004, **51**(11), p 1051-1055.
7. J. Adler, L.-M. Berger, J. Ihle, M. Nebelung, P. Vuoristo, and T. Mantyla, *Non-oxidic Ceramic Coating Powder and Layers Produced Thereform*, WO 03/004718 A2 (2003).
8. B. Wielage, T. Grund, M. Nebelung, S. Thiele, A. Wank, and A. Schwenk, Development and investigation of SiC-based thermal spray powders with alumina-yttria binder matrix, in *Thermal Spray 2007: Global Coating Solutions* (2007), pp. 1140-1144
9. S. Tailor, R.M. Mohanty and P.R. Soni, A Review on Plasma Sprayed Al-SiC Composite Coatings, *J. Mater. Sci. Surf. Eng.*, 2013, **1**(1), p 15-22.
10. B. Torres, M. Campo, A. Urena and J. Rams, Thermal Spray Coatings of Highly Reinforced Aluminium Matrix Composites with sol-gel Silica Coated SiC Particles, *Surf. Coat. Technol.*, 2007, **201**(16-17), p 7552-7559.
11. S. Jiansirisomboon, S.G. Roberts, and P.S. Grant, Low pressure plasma spraying of sol-gel Al_2O_3/SiC nanocomposite coatings, in *Thermal Spray 2001: New Surface for a New Milleninum* (2001), pp. 389-397.
12. M. Tului and T. Valente, *Silicon Carbide Based Thermal Spray Powder, Method of Preparation and Use*, US 20040258916A1 (2004).
13. N. Espallargas and F. Mubarok, *Thermal Spraying of Ceramic Materials,* US20150307980A1 (2012).
14. F. Mubarok and N. Espallargas, Synthesis of thermal spray grade silicon carbide feedstock powder for plasma spray deposition, in *International Thermal Spray Conference* (2015).
15. F. Mubarok, J. Puranen, P. Vuoristo, R. Johnsen, and N. Espallargas, Effect of suspension characteristics on microstructure of suspension plasma sprayed SiC submicron coatings, in *International Thermal Spray Conference 2011* (2011), pp. 756-761.
16. F. Mubarok, S. Armada, I. Fagoaga and N. Espallargas, Thermally Sprayed SiC Coatings for Offshore Wind Turbine Bearing Applications, *J. Therm. Spray Technol.*, 2013, **22**(8), p 1303-1309.
17. F. Mubarok and N. Espallargas, Suspension Plasma Spraying of Sub-micron Silicon Carbide Composite Coatings, *JTST*, 2015, **24**, p 817-825. https://doi.org/10.1007/s11666-015-0242-2
18. F. Mubarok and N. Espallargas, Tribological Behaviour of Thermally Sprayed Silicon Carbide Coatings, *TribologyInternational*, 2015, **85**, p 56-65.
19. www.seramcoatings.com
20. J.R. Davis et al., *Handbook of Thermal Spray Technology*, ASM International, Detroit, 2004.

21. H. Mao, M. Selleby and O. Fabrichnaya, Thermodynamic Reassessment of the Y_2O_3-Al_2O_3-SiO_2 System and Its Subsystems, *Calphad*, 2008, **32**(2), p 399-412.
22. K. Raju and D.-H. Yoon, Sintering Additives for SiC Based on the Reactivity: A Review, *Ceram. Int.*, 2016, **42**(16), p 17947-17962.
23. M. Omori and H. Takei, Pressureless Sintering of SiC, *J. Am. Ceram. Soc.*, 1982, **65**(6), p c92.
24. D.W. Richerson and W.E. Lee, *Modern Ceramic Engineering: Properties, Processing, and Use in Design*, CRC Press, Boca Raton, 2018, p 533-534
25. E.M. Levin and H.F. McMurdie, *Phase Diagrams for Ceramists, 1975 Supplement* (1975).
26. J. Kriegesmann, Processing of Silicon Carbide-Based Ceramics, *Comprehensive Hard Materials*, Vol 2, V. Sarin Ed., Newnes, Oxford, 2014, p 89-175